Nanoscale Advances

ROYAL SOCIETY OF CHEMISTRY

PAPER

View Article Online
View Journal | View Issue

Cite this: *Nanoscale Adv.*, 2020, **2**, 734

A gold nanoparticle-intercalated mesoporous silica-based nanozyme for the selective colorimetric detection of dopamine†

Shounak Ray, Rima Biswas, Rumeli Banerjee and Papu Biswas *

Highly dispersed aggregation-free gold nanoparticles intercalated into the walls of mesoporous silica (AuMS) were synthesized using thioether-functionalized silica as a nanozyme, which exhibited an excellent peroxidase mimic activity. The AuMS material was characterized *via* XRD, N_2 adsorption–desorption, FESEM, SEM-EDS particle mapping, TEM, and XPS. The peroxidase-like activity of the AuMS material was studied thoroughly, and the effect of pH and temperature was evaluated. The reproducibility of the peroxidase mimic activity and long-term stability of the AuMS catalyst were also studied. Furthermore, the AuMS catalyst was successfully utilized for the detection and quantification of dopamine, an important neurotransmitter, colorimetrically with a linear range of 10–80 μM and a limit of detection (LOD) value of 1.28 nM. The determination of dopamine concentration in commercially available dopamine hydrochloride injection showed high accuracy, good reproducibility, and high selectivity in the presence of uric acid, ascorbic acid, glucose, tryptophan, phenylalanine, and tyrosine.

Received 16th August 2019
Accepted 19th December 2019

DOI: 10.1039/c9na00508k

rsc.li/nanoscale-advances

Introduction

In the human body, there exists a perfect balance among biological substances. The imbalance between them could lead to loss of life. Therefore, a specific and selective detection of biological species has arisen as the highest priority to maintain a sustainable life. By utilizing the mechanism of peroxidase activity of HRP, a new and attractive field, which is inspired by nature and aims to imitate natural enzymes using alternative materials, in biomimetic chemistry[1,2] has begun recently and aptly termed as artificial enzymes by Ronald Breslow.[3] Among these artificial enzymes, mostly nanozymes have proved to have the potential to replace natural enzymes by mimicking their activity.[4–6] Also, various advantages of these nanozymes over natural enzymes are that they are (1) cheap and easy to synthesis, (2) robust to harsh environments, (3) stable for a long time, and have (4) large surface area for further modification. The current research trend is focused on nanoenzymes not only because of their enzyme-mimic activity but also because these activities can be tuned to detect biologically relevant materials, such as H_2O_2,[7–10] glucose,[11–15] amino acids *viz.* L-cysteine,[7,14,16] nucleotides,[17] ascorbic acid,[13] melamine,[18] and dopamine,[19] which have vast applications in medicine and other industries.[20–25]

Dopamine (DA) is the most important neurotransmitter present in the human brain and body, whose deficiency causes Parkinson's disease, attention deficit hyperactivity, senile dementia *etc.*[26–28] In the recent years, various techniques such as electrochemical,[29] fluorescence,[30] and LCMS,[31] have been applied for the detection of DA. However, these processes require extensive experimental techniques. Also, the electrochemical detection of DA has one disadvantage of the strong interference from uric acid and ascorbic acid owing to their close voltammetric response.[32] Keeping the fact in mind that UV-vis spectroscopy is still the regularly used analytical tool for the detection of various species in most of the research laboratories, an easy operational colorimetric method for the determination of DA using a simple UV-vis spectrophotometer without any significant interference from UA and AA appeared to be very relevant.

Several groups have reported that nanozymes suffer from poor biocompatibility, toxicity, low activity or selectivity, and complex synthesis procedures despite high stability and tuneability. Moreover, metal nanoparticle-based nanozymes have few inherent shortcomings such as agglomeration, storage difficulty, and poor heterogeneous distribution. Thus, the modification of metal nanoparticles *via* the immobilization of the nanoparticles on a surface having significantly large surface area for the catalytic reaction is one of the possible ways. Immobilization will also eradicate the agglomeration issue to some extent. However, modification with metal nanoparticles often leads to the lowering of the active surface area of the catalyst, and thereby the catalytic activity decreases.[33,34] In this regard, materials based on mesoporous silica have attracted

Department of Chemistry, Indian Institute of Engineering Science and Technology, Shibpur, Howrah 711 103, West Bengal, India. E-mail: papubiswas_besus@yahoo.com

† Electronic supplementary information (ESI) available: Fig. S1–S3. See DOI: 10.1039/c9na00508k

considerable attention due their large surface area, tunable pore size, and feasibility of easy surface modification. Until now very few metal nanoparticle-modified mesoporous silica-based nanozymes have been reported for the detection of biologically relevant substrates. Cu–SBA-15 was reported to demonstrate peroxidase-like activity and utilized to determine H_2O_2.[35] The intrinsic peroxidase-like activity of Fe–SBA-15 microparticles[36] and Fe-grafted mesoporous silica for H_2O_2 and glucose detection have also been reported.[37] This has drawn attention towards noble metal and rare-earth metal nanoparticles, which show some unexpected enzyme-like activity.[38–51]

Recently, in the field of nanozymes, gold nanoparticle-based materials have recently grabbed the prime attention of researchers due to their intrinsic optical and redox properties for use as peroxidase mimicking enzymes.[38–45] Mesoporous silica-encapsulated gold nanoparticles were reported as a glucose oxidase mimick by Ren and Qu *et al.*, collaboratively.[46] Their groups also demonstrated the AuNP growth on mesoporous silica walls, which possess both peroxidase and oxidase activities and used as an efficient antibacterial agent.[47] Recently, dendritic fibrous nano silica-supported gold nanoparticles (DFNS/Au)[48] and thiolated dendritic mesoporous silica nanoparticles loaded with gold nanoparticles (T-DMSN@Au)[49] were also reported as nanozymes capable of mimicking the peroxidase-like activity. Though materials reported so far exhibited good enzymatic behaviour, the reproducibility and long term stability of the catalysts have not been studied thoroughly. We envisioned that utilizing a method to confine the active nanoparticles into the walls of a silica matrix would be an effective route to obtain homogeneously distributed nanoparticles without any agglomeration and pore blocking so that the catalytic activity could be enhanced. Herein, we have demonstrated that the composite of gold nanoparticles intercalated into the walls of mesoporous silica (AuMS) mimicked the peroxidase activity and catalyzed the oxidation of peroxidase substrate 3,3′,5,5′-tetramethylbenzidine (TMB) in the presence of H_2O_2 to generate a blue colour. A selective and sensitive colorimetric method for the determination of dopamine was developed by utilizing the peroxidase-like activity of AuMS, which was successfully used to determine dopamine concentration in a commercially available dopamine hydrochloride injection.

Experimental section

Materials and reagents

The reagents used for the detection of H_2O_2 and dopamine *viz.* 3,3′,5,5′-tetramethylbenzidine (TMB) and dopamine hydrochloride were obtained from Sigma Aldrich. Terephthalic acid, 30% H_2O_2, and NaOH were purchased from Spectrochem, India. Other reagents used for the selectivity study of DA detection *viz.* glucose (Glu), tryptophan (Try), phenylalanine (Phe), tyrosine (Tyr), ascorbic acid (AA) and uric acid (UA) were purchased from TCI. All chemicals were of analytical grade and used without any further purification. A dopamine hydrochloride injection was used as a real sample procured from the hospital medical shop. Aqueous solutions were prepared with Milli-Q double distilled water.

Instrumentation

All the UV-vis colorimetric experiments were performed on an Agilent 8453 diode array spectrophotometer. Fluorescence measurements were studied on a Horiba Fluorolog spectrofluorometer with a 1.0 cm quartz cell (PerkinElmer, USA).

The phase characterization was determined *via* powder X-ray diffraction (XRD) patterns recorded on a Bruker D8 advanced diffractometer with Bragg–Brentano focusing geometry and monochromatic CuK_α radiation ($\lambda = 1.540598$ Å).

The morphological investigations were studied on a JEOL JSM 7610F field-emission scanning electron microscope (FESEM). SEM-EDS spectra were recorded using an Oxford Instruments X-Max^{N}50 X-ray detector attached to a JEOL JSM 7610F scanning electron microscope (SEM). Transmission electron microscopy (TEM) images and selected area electron diffraction (SAED) patterns were recorded using a JEOL JEM-2100 microscope working at 200 kV.

The elemental composition of the catalyst was determined by XPS measurements using a PHI 5000 Versa ProbII, FEI Inc. instrument.

Preparation of gold nano-particles confined in the walls of mesoporous silica

Pluronic P123 (5 g) was dissolved in 375 mL of 2 M HCl in a 500 mL round-bottomed flask at 45 °C. Tetraethyl orthosilicate (TEOS, 10.4 g, 100 mmol) was added dropwise with stirring to the resulting mixture, followed by bis[3-(triethoxysilyl)propyl] tetrasulfide (0.54 g, 1 mmol). An aqueous solution of Au(III) chloride trihydrate (0.39 g, 1 mmol) was subsequently added dropwise to the solution. The stirring was continued for 24 h at 45 °C temperature and aged for 72 h at 100 °C (without stirring). The solid precipitated in the round bottomed flask was filtered off and washed using water thrice, followed washing using ethanol (2 × 30 mL). The resulting solid was dried at 100 °C for 24 h and calcined at 500 °C for 5 h.

Colorimetric H_2O_2 detection

To study the response of AuMS towards peroxidase-like activity, initially, a typical colorimetric experiment was performed in a 0.1 M acetate buffer (pH 4.0) with 2.4 μL TMB (0.125 M in DMSO), which was oxidised by 4 μL of 30% H_2O_2 solution in the presence of 15 μL AuMS (2 mg catalyst dispersed in 1 mL water). The total volume of the solution was kept at 2 mL. UV-vis spectra were recorded at a definite time interval for 5 min, and their corresponding absorbance was plotted against time.

Hydroxyl radical measurements *via* fluorescence spectroscopy

The generation of $OH^\bullet$ was detected through a terephthalic acid photoluminescence probe experiment. 1 mM sodium salt of terephthalic acid (TA) was prepared by dissolving TA into an aqueous solution of NaOH (pH 12). 10 mg AuMS and 10 mM H_2O_2 were incubated in 20 mL acetate buffer (pH 4.0). After the

continuous interval, the solution was centrifuged and used for fluorimetric measurements ($\lambda_{ex} = 315$ nm). A steady increase in the fluorescence intensity at 422 nm was observed with the gradual production of OH˙ radicals.

Colorimetric dopamine detection

For a colorimetric dopamine assay, different amounts of freshly prepared dopamine hydrochloride (DA) solutions (2–100 μM) were introduced in a similar reaction system of total 2 mL as above containing 10 μL TMB (0.125 M in DMSO), 20 μL H_2O_2 in 0.1 M acetate buffer (pH 4.0) in the presence of 15 μL AuMS (2 mg catalyst dispersed in 1 mL water). The solution was incubated at 40 °C for 10 min to generate a blue coloured solution before the addition of DA solutions. The gradual fading of the blue colour of the oxidized TMB upon the addition of DA to the solution was recorded on a UV-vis spectrophotometer at room temperature.

DA determination in the DA hydrochloride injection

For DA determination in the DA hydrochloride injection, first a dopamine injection was procured for a general hospital medical store and diluted 10 times. Then, DA detection was performed with 5 sets of real sample solutions *via* the above procedure.

Results and discussion

Synthesis and characterization of the AuMS catalyst

A one-pot sol–gel method was utilized for the synthesis of AuMS. The incorporation of Au(0) nanoparticles into the wall-framework of SBA-15 was facilitated by the addition of 1,4-bis(triethoxysilyl)propane tetrasulfide (TESPTS) and $HAuCl_4$ during the formation of SBA-15 (Scheme 1).[50] Pure SBA-15 was also prepared under the same condition using both TEOS and TESPTS as the silica sources.

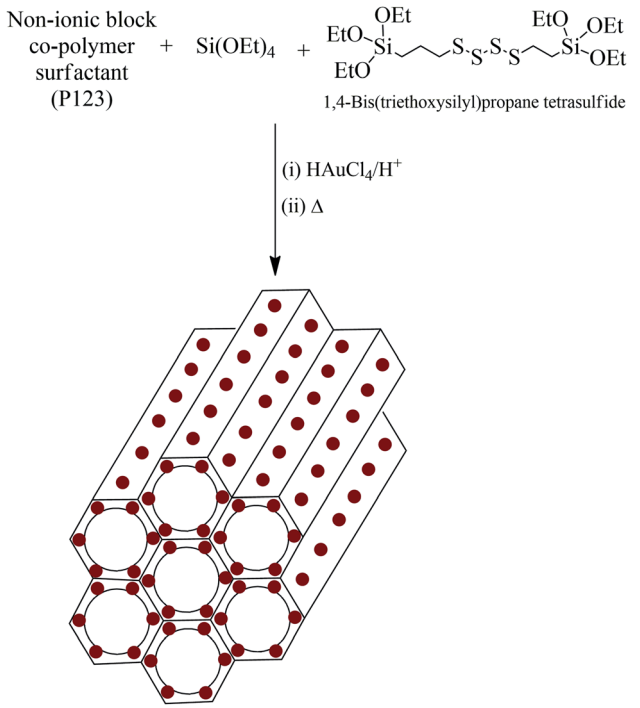

Scheme 1 Formation of mesoporous silica with well-dispersed gold nanoparticles incorporated into the walls of silica (AuMS).

N_2 adsorption–desorption measurements were used to investigate the textural parameters of SBA-15 including BET surface area, pore volume, and pore size distribution (Fig. 1 and Table 1). As shown in Fig. 1a, the nature of nitrogen adsorption isotherms of SBA-15 is type IV with H1-type hysteresis loops, which exhibit a sharp increase at pressures ranging from 0.40–0.8. The nature of isotherms is common for the SBA-15 type of mesoporous silica and confirms the retention of the hexagonal mesoporous structure after the incorporation of Au(0) nanoparticles (AuNPs) into pore walls. The BET surface area and pore volume of the as-prepared sample were found to be 517 $m^2\ g^{-1}$ and 0.68 $cm^3\ g^{-1}$, respectively. SBA-15 prepared under the same condition using TEOS and TESPTS exhibited a BET surface area of 557 $m^2\ g^{-1}$ and a pore volume of 0.74 $cm^3\ g^{-1}$. The BET surface area and pore volume for the samples are almost identical. This indicates that very small AuNPs are mostly incorporated into the pore wall and are not grown inside the pores. The pore size distribution of SBA-15, determined *via* the non-local density functional theory (NLDFT),[51] are displayed in Fig. 1b. The average pore diameters are found to be 5.4 and

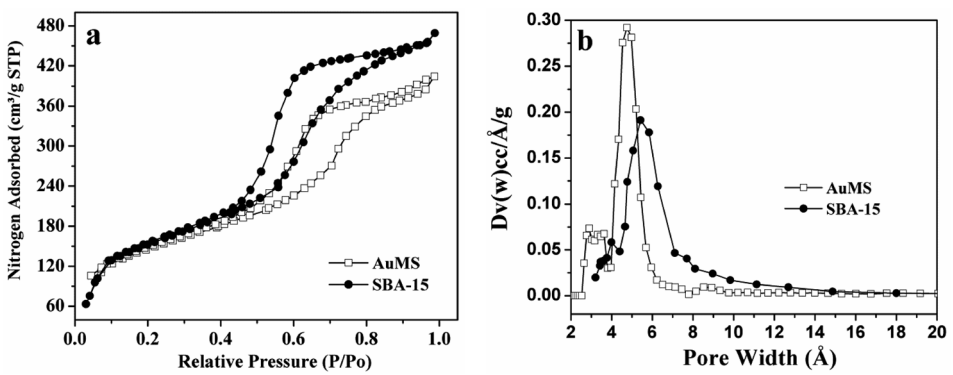

Fig. 1 (a) Physisorption isotherms and (b) corresponding NLDFT pore size distributions of SBA-15 and AuMS.

Table 1 Textural parameters of SBA-15 and AuMS

Samples	BET surface area/m^2 g^{-1}	Pore volume/cm^3 g^{-1}	Pore diameter/nm
SBA-15	557	0.74	5.4
AuMS	516	0.68	4.8

4.8 nm for SBA-15 and AuMS, respectively. A very narrow pore size distribution was found for both the samples.

The crystallinity and phase purity was analyzed *via* wide-angle powder X-ray diffraction, and are shown in Fig. 2. Fig. 2a exhibits the characteristic diffraction peaks at 38.50, 44.72, 64.92, 77.85, 81.91, 98.37, 111.00, 115.48 and 135.54°, corresponding to the (111), (200), (220), (311), (222), (400), (331), (420) and (422) crystal planes of the cubic Au(0) phase ($Fm\bar{3}m$ space group 225) (JCPDS no. 04-0784). The result indicates the formation of pure single-phase AuNPs without any other possible impurities. The broad and weak peaks of AuNPs indicate that the very small Au(0) nanoparticles are highly dispersed. It may be concluded that the confined growth of AuNPs into the walls of mesoporous silica attributes toward small crystalline grain sizes. SBA-15 shows no peak within the range of 20–80° (Fig. 2b).

The morphology of the materials was studied *via* SEM and TEM. As shown in Fig. 3a, short bent rod-like structures with a length of about 1 μm can be observed. The TEM images of SBA-15 are presented in Fig. 3b–d. The hexagonal pores present in AuMS are clearly visible, as shown in Fig. 3c. TEM images (Fig. 3d and e) of the sample reveal well-resolved small nanoparticles within SBA-15. Fig. 1f and g illustrate the HRTEM image of AuNPs located inside the silica framework and corresponding live FFT image, respectively. The SAED pattern of AuNPs (Fig. 3h) shows spots and rings indexed to the (200) and (222) planes of gold with an fcc structure, which is in agreement with the X-ray diffraction studies. The particles into the walls are 3.8 ± 0.5 nm in diameter (Fig. 3e) with an average size of 4 nm (Fig. 4).

The elemental compositions were confirmed by EDS (Fig. S1, see ESI†) and their distributions were further verified by the SEM EDS-mapping results. As shown in Fig. S2, (see ESI†) the elements Si, O and Au exist and distribute uniformly. The content of Au on the SBA-15 was about 2.02 wt%.

The surface composition and electronic structure of AuMS was investigated *via* the XPS analysis. A wide XPS scan of the sample (Fig. 5a) shows the presence of Au, Si and O. The peaks at around 102.1, 154.0 and 531.7 eV could be assigned to Si2p, Si2s, and O1s, respectively. Gold was observed as a small peak at

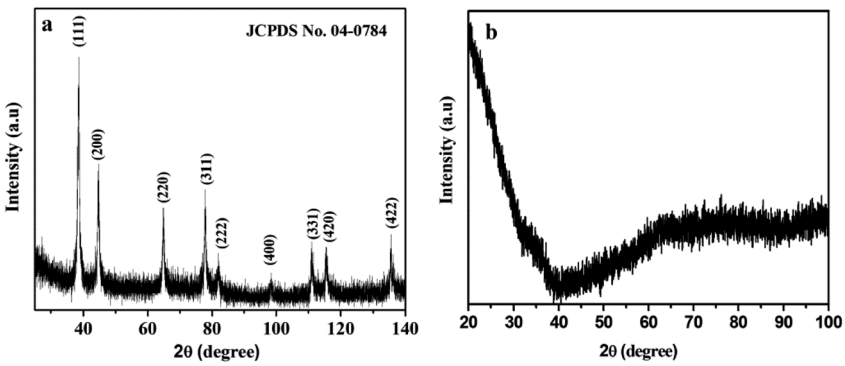

Fig. 2 Wide-angle XRD patterns of (a) AuMS and (b) SBA-15.

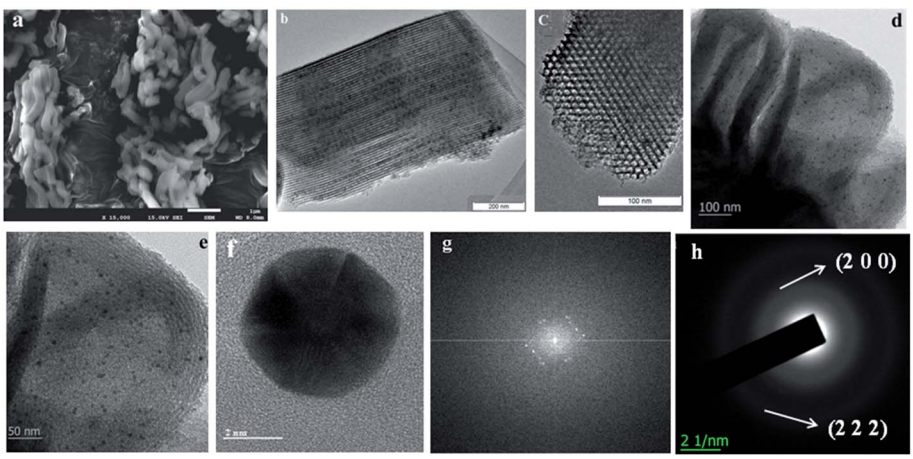

Fig. 3 (a) SEM image of AuMS, (b) TEM image of SBA-15, (c–e) TEM, (f) HRTEM, (g) live FFT and (h) SAED analysis of AuMS.

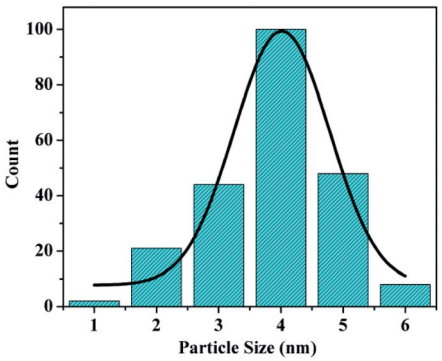

Fig. 4 Particle size distribution of AuMS.

around 85 eV in the surface spectrum (Fig. 5a). The enlarged XPS scan of Au4f (Fig. 5b) demonstrates two peaks at 83.2 eV and 86.8 eV, which are assigned to $Au4f_{7/2}$ and $Au4f_{5/2}$, respectively, and indicates the presence of Au(0). Fig. 5c exhibits a wide XPS scan of SBA-15 (Fig. 5a), which shows the presence of Si and O. The peaks at around 101.9, 153.7 and 531.5 eV are assigned to Si2p, Si2s, and O1s, respectively.

Peroxidase-like activity of AuMS

The peroxidase-like activity of AuMS was studied through the oxidation of 3,3′,5,5′-tetramethylbenzidine (TMB), a typical colorimetric substance that generates blue colour in its oxidized form. The catalytic oxidation of TMB was performed with the assistance of hydrogen peroxide (30% H_2O_2) and AuMS. If the appearance of blue colour in the presence of catalyst follows Michaelis–Menten kinetics, then the catalyst is capable of showing peroxidase mimic activity. The catalytic parameter for a typical enzyme catalytic reaction of the type:

$$E + S = ES$$

$$ES \rightarrow P$$

is obtained from the following Michaelis–Menten equation:

$$V_0 = V_{max}[S]/\{K_M + [S]\}$$

where, E, S, ES, P, V_0, V_{max}, and K_M represent enzyme, substrate, enzyme–substrate adduct, product, initial velocity, maximum reaction velocity, and Michaelis–Menten constant, respectively. V_{max} is attained when the catalytic sites on an enzyme are saturated with the substrate. Another important parameter, *i.e.*, the turnover frequency K_{cat} for an enzyme catalytic reaction is given by the relation $V_{max}/[E]_0$ and catalytic efficiency by the relation K_{cat}/K_M, where $[E]_0$ is the total enzyme (here AuMS) concentration.

Herein, we report the peroxidase-like behavior for AuMS studied through the catalytic oxidation of TMB in the presence

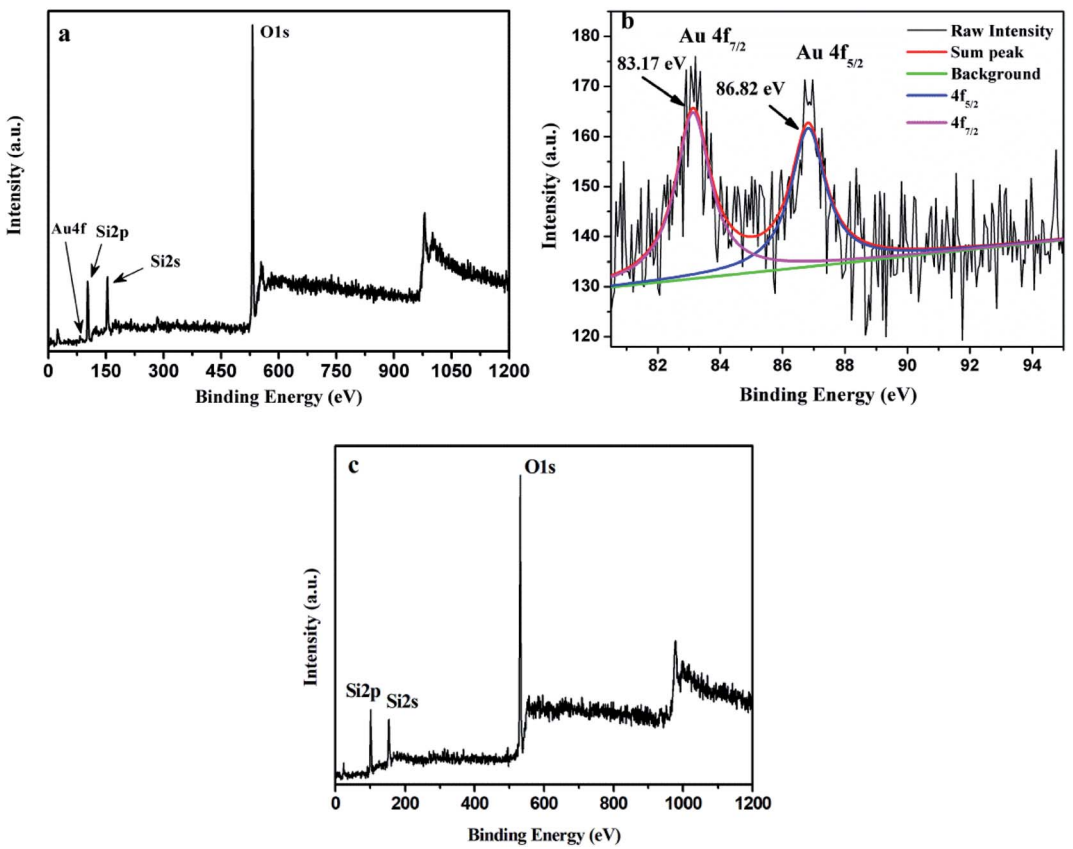

Fig. 5 (a) Wide XPS scan, (b) XPS spectrum of Au4f of AuMS and (c) wide XPS scan of SBA-15 silica.

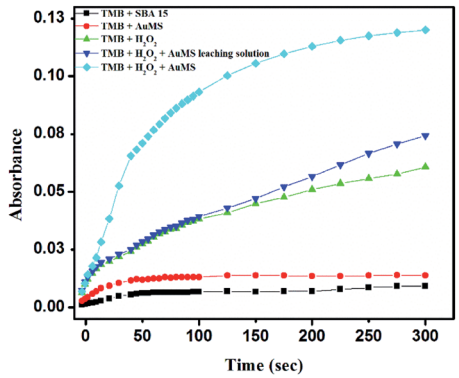

Fig. 6 Time-dependent absorption curve for the TMB–H_2O_2 system using AuMS at 653 nm under different conditions.

of H_2O_2. TMB is chosen as a substrate because it is a non-carcinogenic chromogenic agent. The transformation of colourless TMB to a blue oxidized product having an absorption maxima at 653 nm appears due to the formation of 3,3′,5,5′-tetramethylbenzidine diimine[53] in the presence of AuMS and H_2O_2, proving the peroxidase-like activity of AuMS.

Peroxidase mimicking activity of AuMS

A series of controlled experiments were carried out where the same catalytic reaction was tested with (i) TMB and SBA-15, (ii) TMB and AuMS, (iii) TMB, H_2O_2 and SBA-15, (iv) TMB, H_2O_2 with a AuMS leaching solution and (v) TMB, H_2O_2 and AuMS. Fig. 6 shows the time-dependent absorption curve of AuMS catalyzing the oxidation of TMB. It is evident from Fig. 6 that the absence of H_2O_2 inhibits the oxidation of TMB, while the presence of H_2O_2 shows limited and slow oxidation kinetics even in the presence of bare SBA-15. The only condition for the efficient peroxidase activity is the presence of both catalyst AuMS and H_2O_2. It was also checked that the AuMS leaching solution was unable to show peroxidase activity even in the presence of H_2O_2, indicating that the peroxidase activity is a combined effect of AuMS and H_2O_2. A negligible increase in the activity in the presence of the AuMS leaching solution proves that Au was not leached in the solution when the AuMS dispersion in water was prepared. For the preparation of the AuMS leaching solution, first TMB and AuMS were incubated at 40 °C in a 2 mL acetate buffer (pH = 4). Then, AuMS were centrifuged and separated from the solution. Finally, H_2O_2 was added to the solution before measuring the kinetic study. Thus, the role of AuMS is indispensable as peroxidase mimetic is proven.

Parameter calibration of kinetic reaction

Like a natural peroxidase enzyme HRP, the catalytic activity of AuMS is also effected by temperature and pH. The optimum catalytic condition was studied through varying the reaction pH and temperature. It is seen that the peroxidase activity increases with an increase in pH from 2 to 4, after which it decreases (Fig. 7a). This is probably because TMB is a diamine, which has a poor solubility at a higher pH.[54] Also, the variation of reaction temperature shows that the catalytic activity is optimum at 40 °C, which is also a suitable temperature for natural peroxidase enzymes (Fig. 7b). From the catalyst optimization experiment performed in a similar fashion, (Fig. S3, see ESI†) the amount of catalyst was chosen to be 15 μL (from a stock solution of 2 mg AuMS in 1 mL water). Therefore, it is inferred that AuMS is suitable as a nanozyme for the peroxidase-like activity.

Reproducibility and long-term stability of AuMS

The reproducibility of the proposed catalytic system was tested with the kinetic study of 5 batches of reaction mixtures with AuMS, and the catalytic activity was compared between them in the presence of 40 μL H_2O_2 and 2.4 L μL TMB by performing the kinetic reaction. Nearly similar absorption behavior indicates that AuMS has an excellent reproducibility (Fig. 8a).

The long-term stability of AuMS was tested with a comparison of catalytic activity for the effectiveness of the catalytic oxidation of TMB between freshly prepared AuMS samples with AuMS samples stored for 90 days and found no significant difference of rates between them, which clarifies that the AuMS is highly stable in normal condition (Fig. 8b). It is worth mentioning that AuMS is highly dispersible in water (2 mg mL^{-1}), which helps to improve its catalytic activity.

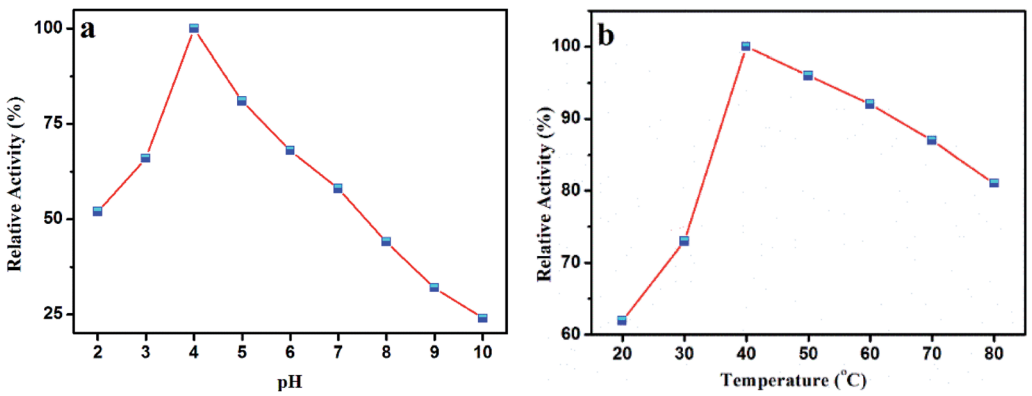

Fig. 7 (a) Effects of pH and (b) temperature on the catalytic oxidation of TMB in the presence of AuMS and H_2O_2.

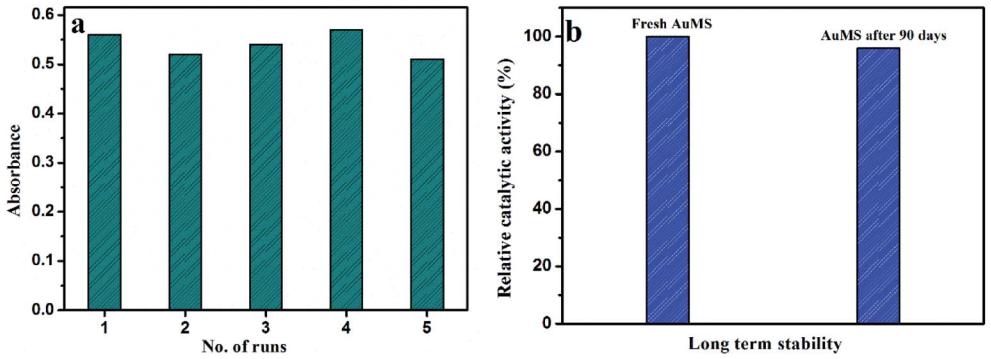

Fig. 8 (a) Reproducibility and (b) long term stability of AuMS as a catalyst.

Kinetics of the TMB oxidation

After a positive response from the catalyst AuMS, two sets of reaction kinetics were obtained to check the concentration dependency over H_2O_2 and TMB. The rate of reaction was estimated from the kinetics of catalysis reaction monitored at a wavelength of 653 nm against reaction time as deep blue colour arises due to the oxidation of TMB with time. In one scenario, the concentration of TMB was fixed at 100 μM, while the concentration of H_2O_2 was varied from the 0 to 42 mM range. In the other case, the concentration of H_2O_2 was kept constant at 13 mM, while the concentration of TMB was varied from 0 to 75 μM. It is clear from Fig. 9 that the reactions follow typical Michaelis–Menten kinetics within a specific range of the substrate concentration. The reaction rates obtained from different sets of reaction kinetics studies were fitted to the Michaelis–Menten equation and Lineweaver–Burk plot to determine the Michaelis–Menten constant, which appears to be 0.146 mM for TMB as substrate and 78.6 mM for H_2O_2 as a substrate, which is substantially a better result as compared to some other gold-catalyzed studies. These values also justify the better binding affinity of AuMS to TMB than the natural peroxidase enzyme HRP (Table 2).

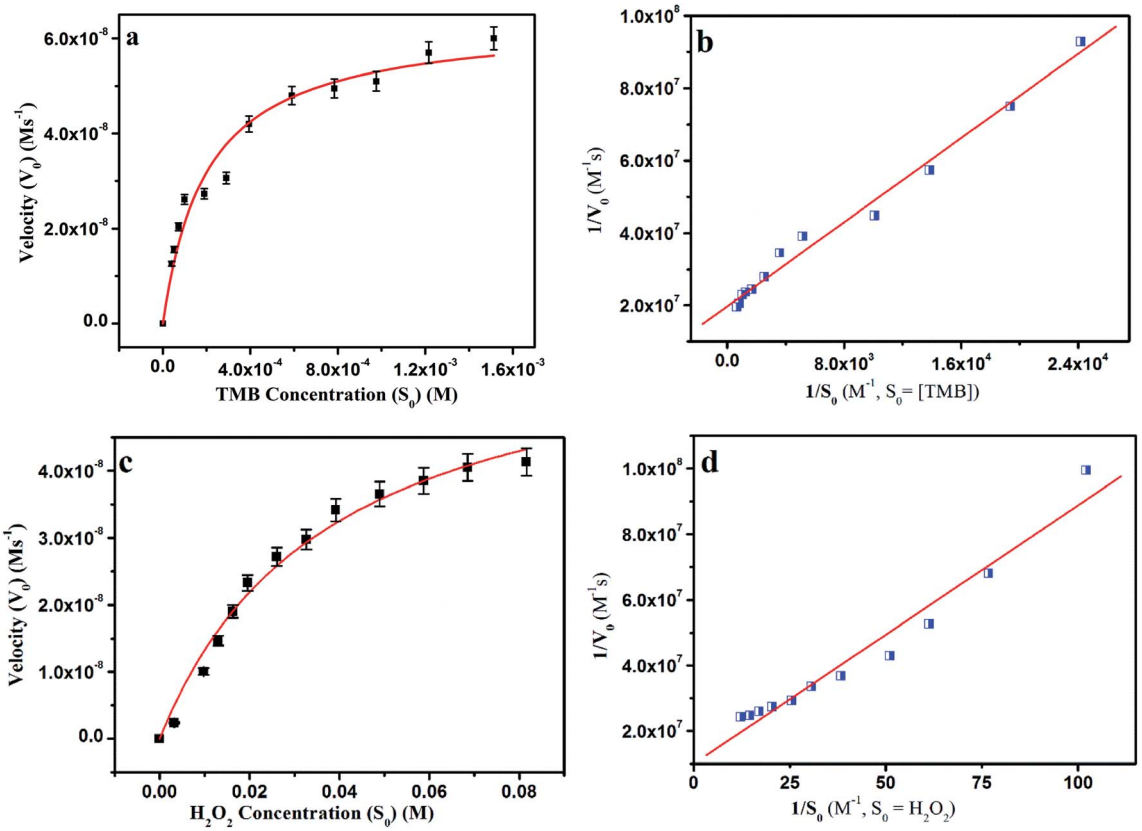

Fig. 9 Steady-state kinetic analyses using the Michaelis–Menten model and Lineweaver–Burk model for AuMS by (a and b) varying the concentration of TMB with a fixed amount of H_2O_2 and (c and d) varying the concentration of H_2O_2 with a fixed amount of TMB.

Table 2 Comparison of K_M and V_{max} of the catalytic oxidation catalyzed by AuMS

Serial no.	Catalyst	Substance	K_M (mM)	V_{max} (M s^{-1})	Ref.
1	EMSN–AuNPs	H_2O_2	119.2	5.25×10^{-8}	46
2	MSN–AuNPs	TMB, H_2O_2	0.0411, 15.81	12.6×10^{-8}, 17.30×10^{-8}	47
3	DFNS/Au-5	TMB	0.220	17.1×10^{-8}	48
4	T-DMSN@Au		0.0407 mM	25.9×10^{-8}	49
5	HRP	TMB, H_2O_2	0.434, 3.7	10×10^{-8}, 8.7×10^{-8}	5
6	AuMS	TMB, H_2O_2	0.146, 78.6	5.07×10^{-8}, 9.9×10^{-8}	This work

Mechanism of the peroxidase-like activity

The mechanism for the peroxidase-like behaviour of nanozymes is well-studied.[52,53] The catalytic process follows a Fenton reaction-like pathway.[19,53–56] In the presence of nanozymes, H_2O_2 decomposed to form a hydroxyl radical (OH˙), which in turn oxidizes TMB to TMB^+ giving rise to blue colour. Due to the high affinity of AuMS towards TMB, the excited electron transfer is promoted and the recombination of electron–hole pairs get hindered, which in turn facilitates the formation of OH˙, resulting in an improved peroxidase-like activity.[57] The mechanism of the reaction was additionally confirmed from the oxidation of terephthalic acid (TA) performed under similar reaction conditions. The acid is a nonfluorescent molecule but in the presence of ˙OH, it converts into an extremely fluorescent 2-hydroxyterephthalic acid (HTA).[13,58] With time, more ˙OH radicals get generated developing more intense fluorescence with time. Thus, the generation of ˙OH radicals and their involvement towards the TMB oxidation in our peroxidase-like activity study has been confirmed (Fig. 10). Since, the gold nanoparticles were confined within the walls of a mesoporous silica matrix, the mesoporous surface of AuMS with more accessible surface area helps the catalytic oxidation of TMB by H_2O_2. It is noteworthy to mention that the catalytic reaction only happens in the simultaneous presence of AuMS, H_2O_2, and

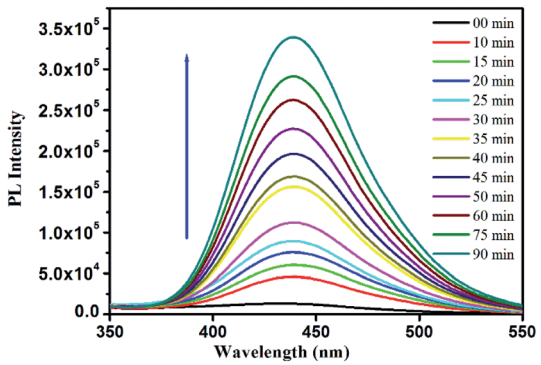

Fig. 10 Fluorescence spectra of the terephthalic acid photoluminescence probe.

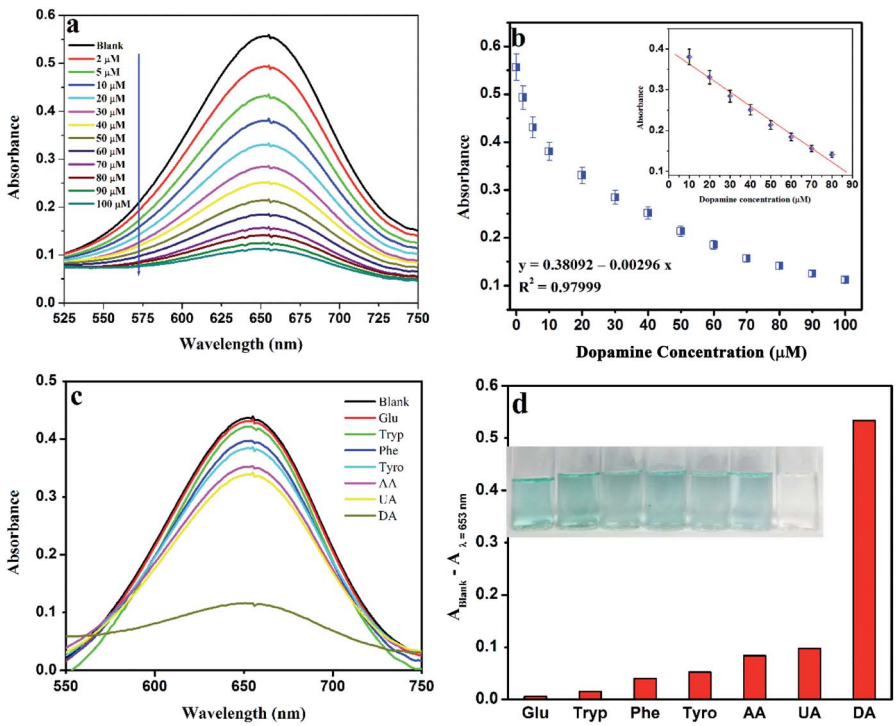

Fig. 11 (a) UV-vis spectra of TMB oxidation in the presence of a variable amount of DA (b) linear calibration plot for DA (c) UV-vis spectra of TMB oxidation in the presence of 100 μM various interfering species, and (d) comparison with other substrates.

Table 3 Application of the proposed assay for the detection of DA in real samples

Sample	Without spiking (μM)	DA spiked (μM)	DA measured (μM)	Recovery (%)
Injection 1	17.21 ± 0.89	5	22.44 ± 0.42	104.6
Injection 2	14.87 ± 0.77	10	24.58 ± 0.61	97.1
Injection 3	22.34 ± 0.57	15	37.85 ± 0.26	103.4
Injection 4	11.58 ± 0.72	20	30.82 ± 0.21	96.2
Injection 5	7.29 ± 0.63	25	32.65 ± 0.37	101.4

TMB. The absence of any of the component fails to exhibit blue colouration.

Detection of dopamine

The excellent peroxidase behavior tempted us to see if any other colorimetric application could be developed for the detection of an important biologically active species. A facile and sensitive colorimetric sensor for DA is fabricated depending on the fact that due to the presence of the reducing ability of dopamine, the amino and phenol hydroxyl groups of DA consume H_2O_2 *via* redox reaction, which leads to the inhibition of the oxidation of TMB, showing a blue colour fade and decreasing the absorbance intensity at 653 nm.[59] Simultaneously, the electro-active nature of DA favours its oxidation into dopamine-*o*-quinine by H_2O_2 over TMB.[60,61] Under optimized conditions, this quenching of blue colour is recorded on a UV-vis spectrophotometer with the gradual addition of DA into the reaction mixture containing TMB, AuMS and H_2O_2 in a fixed concentration in the acetate buffer solution (pH 4).

With the gradual addition of a set of different concentrations of DA into the reaction system, the absorption intensity at 653 nm decreases, which is also recognizable through naked eye clearly (Fig. 11a and b). A linear relationship is established between absorbance *vs.* concentration within the range of 10–80 μM ($R^2 = 0.9799$) with a LOD of 1.28 nM (S/N = 3.3). The linear range and LOD value are comparable with previously reported values.[62,63] The wide linear range favours this system for medical and clinical applications also.

The selectivity of the proposed system was investigated in the presence of various interfering species, which are also present along with DA in the human body, such as glucose (Glu), tryptophan (Try), phenylalanine (Phe), tyrosine (Tyr), ascorbic acid (AA) and uric acid (UA) in place of DA. From Fig. 11c, it is clearly evident that only DA has the ability to inhibit the oxidation of TMB, thereby quenching the blue color efficiently. The high selectivity towards DA is observed from the bar diagram (Fig. 11d) plot of the difference of the absorbance value at 653 nm in the absence and presence of investigated molecules. The photographic images clearly indicate the efficiency from a naked eye view.

Detection of dopamine in the DA injection

The sensitivity of the proposed system was checked with a real sample analysis. For the real sample analysis, a DA injection was procured from a chemist shop, and the AuMS + TMB + H_2O_2 system was applied to see the blue colour fade in UV-vis spectrophotometer along with the detection of DA. The results are recorded in Table 3 and recovery were calculated, which shows that the proposed system is highly suitable for clinical applications also.

Conclusion

In summary, AuNPs were intercalated into the walls of mesoporous silica *via* a one-step sol–gel process, and this was confirmed from the BET analysis. Pure SBA-15 and AuMS exhibited almost the same surface area of 557 and 517 $m^2\ g^{-1}$, respectively, as revealed *via* the BET measurements, which validate the fact of incorporation of AuNPs mostly into the walls of mesoporous silica. The presence of pure metallic gold with a face-centered cubic lattice was confirmed from the XRD analysis. Two individual binding energies obtained in the XPS analysis for $Au4f_{7/2}$ and $Au4f_{5/2}$ further strengthened the presence of metallic gold. The HRTEM analysis confirms the average size of the intercalated AuNPs to be 4 nm. AuMS shows an excellent enzymatic peroxidase-like activity using 3,3′,5,5′-tetramethylbenzidine (TMB) as a model substrate, and the K_M and V_{max} values observed are better than those of natural enzyme HRP. However, the presence of dopamine (DA) inhibited the formation of oxTMB and based on that a sensitive and selective colorimetric DA detection probe was successfully achieved. The colorimetric DA detection assay has a linear range of 10–80 μM with a LOD of 1.28 nM. The proposed sensor was also tested for the detection of DA in the dopamine hydrochloride injection sample very efficiently.

Conflicts of interest

The authors declare no competing financial interest.

Acknowledgements

Rima Biswas acknowledges UGC-India for providing NFSC Fellowship (F1-17.1/2017-18/RGNF-2017-18-SC-WES-40353/SA-III/Website). Rumeli Banerjee acknowledges DST-INSPIRE, India for providing INSPIRE Fellowship (IF 160999).

References

1 R. Breslow, *Artificial enzymes*, Wiley-VCH, Weinheim, 2005.

2 A. J. Kirby and F. Hollfelder, *From enzyme models to model enzymes*, Royal Society of Chemistry, Cambridge, 2009.
3 R. Breslow and L. E. Overman, "Artificial enzyme" combining a metal catalytic group and a hydrophobic binding cavity, *J. Am. Chem. Soc.*, 1970, **92**, 1075–1077.
4 H. Wei and E. Wang, Nanomaterials with enzyme-like characteristics (nanozymes): next-generation artificial enzymes, *Chem. Soc. Rev.*, 2013, **42**, 6060–6093.
5 L. Gao, J. Zhuang, L. Nie, J. Zhang, Y. Zhang, N. Gu, T. Wang, J. Feng, D. Yang, S. Perrett and X. Yan, Intrinsic peroxidase-like activity of ferromagnetic nanoparticles, *Nat. Nanotechnol.*, 2007, **2**, 577–583.
6 Y. Song, K. Qu, C. Zhao, J. Ren and X. Qu, Graphene oxide: intrinsic peroxidase catalytic activity and its application to glucose detection, *Adv. Mater.*, 2010, **22**, 2206–2210.
7 C. Ray, S. Dutta, S. Sarkar, R. Sahoo, A. Roy and T. Pal, Intrinsic peroxidase-like activity of mesoporous nickel oxide for selective cysteine sensing, *J. Mater. Chem. B*, 2014, **2**, 6097–6105.
8 M. Aghayan, A. Mahmoudi, M. Reza Sazegar, N. Ghavidel Hajiagh and K. Nazari, Enzymatic activity of Fe-grafted mesoporous silica nanoparticles: an insight into H2O2 and glucose detection, *New J. Chem.*, 2018, **42**, 16060–16068.
9 Z. Zhang, J. Hao, W. Yang, B. Lu, X. Ke, B. Zhang and J. Tang, Porous Co3O4 nanorods–reduced graphene oxide with intrinsic peroxidase-like activity and catalysis in the degradation of methylene blue, *ACS Appl. Mater. Interfaces*, 2013, **5**, 3809–3815.
10 T. Wang, Y. Fu, L. Chai, L. Chao, L. Bu, Y. Meng, C. Chen, M. Ma, Q. Xie and S. Yao, Filling carbon nanotubes with prussian blue nanoparticles of high peroxidase–like catalytic activity for colorimetric chemo– and biosensing, *Chem.–Eur. J.*, 2014, **20**, 2623–2630.
11 L. Artiglia, S. Agnoli, M. C. Paganini, M. Cattelan and G. Granozzi, TiO_2@CeO_x Core–shell nanoparticles as artificial enzymes with peroxidase-like activity, *ACS Appl. Mater. Interfaces*, 2014, **6**, 20130–20136.
12 S. Dutta, S. Sarkar, C. Ray and T. Pal, Benzoin derived reduced graphene oxide (rGO) and its nanocomposite: application in dye removal and peroxidase-like activity, *RSC Adv.*, 2013, **3**, 21475–21483.
13 H. Tan, C. Ma, L. Gao, Q. Li, Y. Song, F. Xu, T. Wang and L. Wang, Metal–organic framework–derived copper nanoparticle@carbon nanocomposites as peroxidase mimics for colorimetric sensing of ascorbic acid, *Chem.–Eur. J.*, 2014, **20**, 16377–16383.
14 X. Zheng, Q. Zhu, H. Song, X. Zhao, T. Yi, H. Chen and X. Chen, In situ synthesis of self-assembled three-dimensional graphene–magnetic palladium nanohybrids with dual-enzyme activity through one-pot strategy and its application in glucose probe, *ACS Appl. Mater. Interfaces*, 2015, **7**, 3480–3491.
15 A. K. Dutta, S. Das, S. Samanta, P. K. Samanta, B. Adhikary and P. Biswas, CuS nanoparticles as a mimic peroxidase for colorimetric estimation of human blood glucose level, *Talanta*, 2013, **107**, 361–367.
16 L. Zhan, C. M. Li, W. B. Wu and C. Z. Huang, A colorimetric immunoassay for respiratory syncytial virus detection based on gold nanoparticles–graphene oxide hybrids with mercury-enhanced peroxidase-like activity, *Chem. Commun.*, 2014, **50**, 11526–11528.
17 Y. Song, X. Wang, C. Zhao, K. Qu, J. Ren and X. Qu, Label–free colorimetric detection of single nucleotide polymorphism by using single–walled carbon nanotube intrinsic peroxidase–like activity, *Chem.–Eur. J.*, 2010, **16**, 3617–3621.
18 N. Ding, N. Yan, C. Ren and X. Chen, Colorimetric determination of melamine in dairy products by Fe3O4 magnetic nanoparticles−H2O2−ABTS detection system, *Anal. Chem.*, 2010, **82**, 5897–5899.
19 S. Dutta, C. Ray, S. Mallick, S. Sarkar, R. Sahoo, Y. Negishi and T. Pal, A gel-based approach to design hierarchical CuS decorated reduced graphene oxide nanosheets for enhanced peroxidase-like activity leading to colorimetric detection of dopamine, *J. Phys. Chem. C*, 2015, **119**, 23790–23800.
20 A. A. Vernekar, T. Das, S. Ghosh and G. Mugesh, A remarkably efficient MnFe2O4–based oxidase nanozyme, *Chem.–Asian J.*, 2016, **11**, 72–76.
21 H. Cheng, L. Zhang, J. He, W. Guo, Z. Zhou, X. Zhang, S. Nie and H. Wei, Integrated nanozymes with nanoscale proximity for in vivo neurochemical monitoring in living brains, *Anal. Chem.*, 2016, **88**, 5489–5497.
22 X. Wang, Y. Hu and H. Wei, Nanozymes in bionanotechnology: from sensing to therapeutics and beyond, *Inorg. Chem. Front.*, 2016, **3**, 41–60.
23 K. M. Koeller and C. H. Wong, Enzymes for chemical synthesis, *Nature*, 2001, **409**, 232–240.
24 B. Liu, Z. Sun, P. J. J. Huang and J. Liu, Hydrogen peroxide displacing DNA from nanoceria: mechanism and detection of glucose in serum, *J. Am. Chem. Soc.*, 2015, **137**, 1290–1295.
25 M. S. Hizir, M. Top, M. Balcioglu, M. Rana, N. M. Robertson, F. Shen, J. Sheng and M. V. Yigit, Multiplexed activity of peroxidase: DNA-capped AuNPs act as adjustable peroxidase, *Anal. Chem.*, 2016, **88**, 600–605.
26 A. Zhang, J. L. Neumeyer and R. J. Baldessarini, Recent progress in development of dopamine receptor subtype-selective agents: potential therapeutics for neurological and psychiatric disorders, *Chem. Rev.*, 2007, **107**, 274–302.
27 T. M. Dawson and V. L. Dawson, Molecular pathways of neurodegeneration in parkinson's disease, *Science*, 2003, **302**, 819–822.
28 C. J. Hong, H. C. Liu, T. Y. Liu, D. L. Liao and S. J. Tsai, Association studies of the adenosine A2a receptor (1976T > C) genetic polymorphism in Parkinson's disease and schizophrenia, *J. Neural Transm.*, 2005, **112**, 1503–1510.
29 L. Zhang, L. Ning, S. Li, H. Pang, Z. Zhang, H. Ma and H. Yan, Selective electrochemical detection of dopamine in the presence of uric acid and ascorbic acid based on a composite film modified electrode, *RSC Adv.*, 2016, **6**, 66468–66476.
30 M. Ganguly, C. Mondal, J. Jana, A. Pal and T. Pal, Selective dopamine chemosensing using silver-enhanced fluorescence, *Langmuir*, 2014, **30**, 4120–4128.

31 V. Carrera, E. Sabater, E. Vilanova and M. A. Sogorb, A simple and rapid HPLC–MS method for the simultaneous determination of epinephrine, norepinephrine, dopamine and 5-hydroxytryptamine: Application to the secretion of bovine chromaffin cell cultures, *J. Chromatogr. B: Anal. Technol. Biomed. Life Sci.*, 2007, **847**, 88–94.

32 Z. Guo, M.-L. Seol, M.-S. Kim, J.-H. Ahn, Y.-K. Choi, J.-H. Liu and X.-J. Huang, Sensitive and selective electrochemical detection of dopamine using an electrode modified with carboxylated carbonaceous spheres, *Analyst*, 2013, **138**, 2683–2690.

33 X. M. Shen, W. Q. Liu, X. J. Gao, Z. H. Lu, X. C. Wu and X. F. Gao, Mechanisms of oxidase and superoxide dismutation-like activities of gold, silver, platinum, and palladium, and their alloys: a general way to the activation of molecular oxygen, *J. Am. Chem. Soc.*, 2015, **137**, 15882–15891.

34 S. Wang, W. Chen, A. L. Liu, L. Hong, H. H. Deng and X. H. Lin, Comparison of the peroxidase-like activity of unmodified, amino-modified, and citrate-capped gold nanoparticles, *ChemPhysChem*, 2012, **13**, 1199–1204.

35 J. Mu, Y. He and Y. Wang, Copper-incorporated SBA-15 with peroxidase-like activity and its application for colorimetric detection of glucose in human serum, *Talanta*, 2016, **148**, 22–28.

36 S. Liu, J. Tian, L. Wang, Y. Luo, G. Chang and X. Sun, Iron-substituted SBA-15 microparticles: a peroxidase-like catalyst for H_2O_2 detection, *Analyst*, 2011, **136**, 4894–4897.

37 M. Aghayan, A. Mahmoudi, M. Reza Sazegar, N. G. Hajiaghaa and K. Nazarib, Enzymatic activity of Fe-grafted mesoporous silica nanoparticles: an insight into H2O2 and glucose detection, *New J. Chem.*, 2018, **42**, 16060–16068.

38 L. Pasquato, F. Rancan, P. Scrimin, F. Mancin and C. Frigeri, N-Methylimidazole-functionalized gold nanoparticles as catalysts for cleavage of a carboxylic acid ester, *Chem. Commun.*, 2000, 2253–2254.

39 F. Manea, F. B. Houillon, L. Pasquato and P. Scrimin, Nanozymes: gold-nanoparticle-based transphosphorylation catalysts, *Angew. Chem., Int. Ed.*, 2004, **43**, 6165–6169.

40 M. Comotti, C. Della Pina, R. Matarrese and M. Rossi, The catalytic activity of "naked" gold particles, *Angew. Chem., Int. Ed.*, 2004, **43**, 5812–5815.

41 P. Beltrame, M. Comotti, C. Della Pina and M. Rossi, Aerobic oxidation of glucose: II. catalysis by colloidal gold, *Appl. Catal., A*, 2006, **297**, 1–7.

42 J. Y. Feng, P. C. Huang and F. Y. Wu, Gold-platinum bimetallic nanoclusters with enhanced peroxidase-like activity and their integrated agarose hydrogel-based sensing platform for the colorimetric analysis of glucose levels in serum, *Analyst*, 2017, **142**, 4106–4115.

43 Y. Tao, Y. H. Lin, Z. Z. Huang, J. S. Ren and X. G. Qu, Incorporating graphene oxide and gold nanoclusters: a synergistic catalyst with surprisingly high peroxidase–like activity over a broad pH range and its application for cancer cell detection, *Adv. Mater.*, 2013, **25**, 2594–2599.

44 W. Song, G. D. Nie, W. Ji, Y. Z. Jiang, X. F. Lu, B. Zhao and Y. Ozaki, Synthesis of bifunctional reduced graphene oxide/CuS/Au composite nanosheets for in situ monitoring of a peroxidase-like catalytic reaction by surface-enhanced Raman spectroscopy, *RSC Adv.*, 2016, **6**, 54456–54462.

45 W. He, Y. Liu, J. Yuan, J.-J. Yin, X. Wu, X. Hu, K. Zhang, J. Liu, C. Chen, Y. Ji and Y. Guo, Au@Pt nanostructures as oxidase and peroxidase mimetics for use in immunoassays, *Biomaterials*, 2011, **32**, 1139–1147.

46 Y. Lin, Z. Li, Z. Chen, J. Ren and X. Qu, Mesoporous silica-encapsulated gold nanoparticles as artificial enzymes for self-activated cascade catalysis, *Biomaterials*, 2013, **34**, 2600–2610.

47 Y. Tao, E. Ju, J. Ren and X. Qu, Bifunctionalized mesoporous silica-supported gold nanoparticles: intrinsic oxidase and peroxidase catalytic activities for antibacterial applications, *Adv. Mater.*, 2015, **27**, 1097–1104.

48 R. Singh, R. Belgamwar, M. Dhiman and V. Polshettiwar, Dendritic fibrous nano-silica supported gold nanoparticles as an artificial enzyme, *J. Mater. Chem. B*, 2018, **6**, 1600–1604.

49 M. Kalantari, T. Ghosh, Y. Liu, J. Zhang, J. Zou, C. Lei and C. Yu, Highly thiolated dendritic mesoporous silica nanoparticles with high-content gold as nanozymes: the nano-gold size matters, *ACS Appl. Mater. Interfaces*, 2019, **11**, 13264–13272.

50 L. Chen, J. Hu and R. Richards, Intercalation of aggregation-free and well-dispersed gold nanoparticles into the walls of mesoporous silica as a robust "green" catalyst for n-alkane oxidation, *J. Am. Chem. Soc.*, 2009, **131**, 914–915.

51 P. I. Ravikovitch and A. V. Neimark, Characterization of micro- and mesoporosity in SBA-15 materials from adsorption data by the NLDFT method, *J. Phys. Chem. B*, 2001, **105**, 6817–6823.

52 M. G. Zhao, J. Y. Huang, Y. Zhou, X. H. Pan, H. P. He, Z. Z. Ye and X. Q. Pan, Controlled synthesis of spinel $ZnFe_2O_4$ decorated ZnO heterostructures as peroxidase mimetics for enhanced colorimetric biosensing, *Chem. Commun.*, 2013, **49**, 7656–7658.

53 X. F. Lu, X. J. Bian, Z. C. Li, D. M. Chao and C. Wang, A facile strategy to decorate Cu_9S_5 nanocrystals on polyaniline nanowires and their synergetic catalytic properties, *Sci. Rep.*, 2013, **13**, 2955.

54 Q. Cai, S. K. Lu, F. Liao, Y. Q. Li, S. Z. Ma and M. W. Shao, Catalytic degradation of dye molecules and in situ SERS monitoring by peroxidase-like Au/CuS composite, *Nanoscale*, 2014, **6**, 8117–8123.

55 L. Zhang, X. Hai, C. Xia, X. W. Chen and J. H. Wang, Growth of CuO nano needles on graphene quantum dots as peroxidase mimics for sensitive colorimetric detection of hydrogen peroxide and glucose, *Sens. Actuators, B*, 2017, **248**, 374–384.

56 A. Zeb, X. Xie, A. B. Yousaf, M. Imran, T. Wen, Z. Wang, H. L. Guo, Y. F. Jiang, I. A. Qazi and A. W. Xn, Highly Efficient Fenton and Enzyme-Mimetic Activities of Mixed-Phase VOx Nanoflakes, *ACS Appl. Mater. Interfaces*, 2016, **8**, 30126–30132.

57 Y. Ma, M. G. Zhao, B. Cai, W. Wang, Z. Z. Ye and J. Y. Huang, 3D graphene network@WO_3 nanowire composites: a multifunctional colorimetric and electrochemical

biosensing platform, *Chem. Commun.*, 2014, **50**, 11135–11138.

58 W. Chen, J. Chen, Y. B. Feng, L. Hong, Q. Y. Chen, L. F. Wu, X. H. Lin and X. H. Xia, Peroxidase-like activity of water-soluble cupric oxide nanoparticles and its analytical application for detection of hydrogen peroxide and glucose, *Analyst*, 2012, **137**, 1706–1712.

59 J. Mu, Y. Wang, M. Zhao and L. Zhang, Intrinsic peroxidase-like activity and catalase-like activity of Co_3O_4 nanoparticles, *Chem. Commun.*, 2012, **48**, 2540–2542.

60 M. Hosseini, M. Aghazadeh and M. R. Ganjali, A facile one-pot synthesis of cobalt-doped magnetite/graphene nanocomposite as peroxidase mimetics in dopamine detection, *New J. Chem.*, 2017, **41**, 12678–12684.

61 B. Somturk, M. Hancer, I. Ocsoy and N. Özdemir, Synthesis of copper ion incorporated horseradish peroxidase-based hybrid nanoflowers for enhanced catalytic activity and stability, *Dalton Trans.*, 2015, **44**, 13845–13852.

62 J.-J. Feng, H. Guo, Y.-F. Li, Y.-H. Wang, W.-Y. Chen and A.-J. Wang, Single molecular functionalized gold nanoparticles for hydrogen-bonding recognition and colorimetric detection of dopamine with high sensitivity and selectivity, *ACS Appl. Mater. Interfaces*, 2013, **5**, 1226–1231.

63 T.-Q. Xu, Q.-L. Zhang, J.-N. Zheng, Z.-Y. Lv, J. Wei, Ai.-J. Wang and J.-J. Feng, Simultaneous determination of dopamine and uric acid in the presence of ascorbic acid using Pt nanoparticles supported on reduced graphene oxide, *Electrochim. Acta*, 2014, **115**, 109–115.